Journal of Materials Chemistry A

Accepted Manuscript

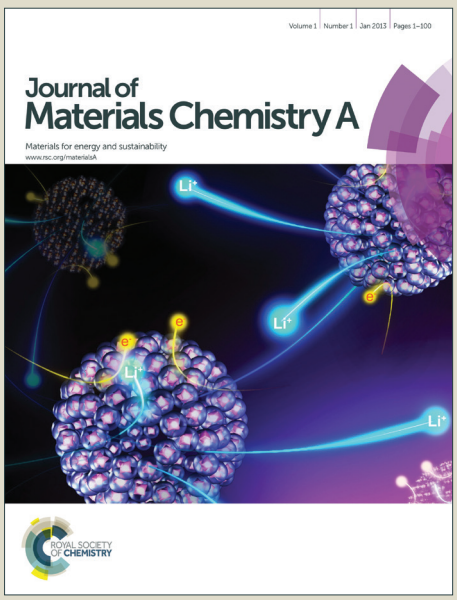

ROYAL SOCIETY OF CHEMISTRY

www.rsc.org/materialsA

Journal of Materials Chemistry A RSCPublishing

ARTICLE

Effects of the Mesostructural Order on the Electrochemical Performance of Hierarchical Micro-Mesoporous Carbons

Cite this: DOI: 10.1039/x0xx00000x

Received ooth January 2012,
Accepted ooth January 2012

DOI: 10.1039/x0xx00000x

www.rsc.org/

M. Enterría*[a],A. Castro-Muñiz [b],F. Suárez-García [a], A. Martínez-Alonso [a] ,J.M.D. Tascón [a] and T. Kyotani [b].

Hierarchical ordered porous carbons show better behavior as electric double layer capacitors (EDLCs) than disordered carbons especially at high rates thanks to their unique architectural design. In the present work, we demonstrate that mesostructural order is a key factor for the performance of carbons at high rates. For that, two series of hierarchical micro-mesoporous carbons were prepared by chemical activation with KOH following two different procedures. SBA-15 silica was infiltrated by chemical vapor deposition of propylene and the resulting carbon/silica composite was split in two halves. One part was directly activated and, subsequent to activation process, the template was eliminated. The second part was firstly subjected to the template removal and, the resulting CMK-3 type carbon was further activated. Thus, carbons obtained by both methods present bimodal pore size distributions and different mesostructural order as a function of the activation conditions. Carbons prepared from the direct activations of the composite present a high conservation of the ordered mesoporous structure. The electrochemical performance of both carbon series was tested in acid aqueous electrolyte (1M H_2SO_4) by cyclic voltammetry and impedance spectroscopy. A highly ordered mesoporous structure significantly improves the specific capacitance at high scan rates due to enhancement the diffusion of molecules.

1. Introduction

Supercapacitors or electric double layer capacitors (EDLCs) have attracted much attention in the field of energy storage due to their high power density, fast recharge capability and long cycle life.[1] It is widely demonstrated[2-10] that high surface area, presence of mesopores and appropriate pore size distributions in the EDLCs electrodes are necessary for a high electrochemical performance. The importance of mesopores for increasing the diffusion of the solvated ions had been pointed out in many works[4, 6, 10, 11] and the enhanced performance of hierarchical materials in this application was also demonstrated.[4, 7, 11-13] Thus, high surface area carbons containing regularly interconnected micro and mesopores are thought to have potential as EDLC electrodes since charge storage and rate capability are strongly limited if the pores are randomly connected.[7] Hypothetically, when the specific surface area of the carbon increases so does its capacitance,[8, 10, 14] but in fact, the pore accessibility is a key factor.[10] Micropores play an important role in terms of capacitance enhancement, but except for ordered micropores in the zeolite template carbons,[15] they limit the fast diffusion of electrolytes. This is a big drawback since, for normal usage conditions of electrodes, fast scans and current densities are demanded.

In activated carbons, the pathway which solvated ions have to go through in order to reach micropores is very complex and long. Mesoporous carbons, having an adjustable and interconnected ordered mesopore network, are thought to enhance ionic transport since the solvated ions are expected to diffuse easily through ordered mesoporous channels to the micropores. Thus, different authors have demonstrated the influence of the ordered mesopore structure of carbons prepared by templating technique on the capacity of EDLC electrodes working at high rates.[7, 16-20] Furthermore, the influence of the mesopore symmetry and structure has been demonstrated as well.[16-18, 21]The main disadvantage of ordered mesoporous carbons (OMCs) is their modest surface area. Their micropore volume can be improved by means of both chemical and physical activation,[11-13, 22-30] but it is increased at the expense of the ordered mesoporous structure.[18, 22-24, 31] In the case of OMCs prepared using mesoporous silicas as template (hard-templating technique), our research group has demonstrated that activation of carbons in the presence of the template (i.e. activation of the carbon/silica composite) preserves the

structural order, even under strong activation conditions (high temperatures and high KOH/precursor ratios) and high micropore volumes are developed while the silica provides protection to the mesostructure.[23] The aim of this work is to investigate the influence of the mesoporous structure order on the electrochemical performance. To this aim, cyclic voltammetry and electrochemical impedance spectroscopy of two different series of activated OMCs are compared for i) one carbon series with a rather deteriorated mesostructure due to the chemical activation process[22] and ii) another series with high preservation of the mesostructural order.[23]

2. Experimental

2.1. Carbon preparation

The preparation and activation conditions for the OMCs were reported in detail in previous works from our group.[22, 23] Briefly, SBA-15 mesoporous silica was infiltrated by chemical vapor deposition of propylene in argon (5.5% v/v) at 750 ºC for 6 h and then carbonized at 950 ºC for 2 h under argon atmosphere. The resulting carbon/silica composite (having an infiltration degree of 55 wt.%, measured by thermogravimetric analysis in air at 950 ºC), was split in two halves. One part was directly activated and, subsequent to the activation process, the template was eliminated. To this end, the carbon/silica composite was physically mixed with different amounts of KOH (KOH/OMC weight ratios of 2/1, 4/1and 8/1) and carbonized under argon up to 750 or 850 ºC for 30 min. The resulting activated composites were washed with HCl (1 M) and distilled water for removing the activating agent. Finally, the silica template was removed with HF (48%, Merck) and the resulting OMC was filtered and repeatedly washed with water and dried.

The second half of the carbon/silica composite was firstly subjected to template removal with HF, the resulting CMK-3 type carbon was then activated following the same activation/washing conditions as indicated previously for the composites but using KOH/OMC weight ratios of 2/1 and 4/1.Carbons resulting from activation after template removal were named as CX1-T (C series), whereas carbons activated in template presence were named as CBX1-T (CB series). X stands for the KOH/carbon mass ratio (2, 4 or 8) and T stands for the activation temperature (750 or 850 ºC). The amount of ash (i.e. remaining silica template and residues from activation) in the final carbons after etching and washing was < 1 wt.%, measured by TG in air at 900ºC.

2.2. Textural characterization

An Autosorb-1 (Quantachrome) volumetric adsorption analyzer was used to measure N_2 (purity > 99.999%) adsorption-desorption isotherms at -196 ºC in the 10^{-7} – 0.99 relative pressure range. Adsorption isotherms of CO_2 (purity > 99.98%) at 0 ºC in the 10^{-5} – 0.03 relative pressure range were measured in a semiautomatic adsorption apparatus (Nova-1200, Quantachrome). Prior to the adsorption measurements, the samples were degassed overnight at 250 ºC under vacuum. The BET surface area (S_{BET}) was calculated according to the BET model[32] from the nitrogen isotherms in the relative pressure range of 0.05 - 0.25. The micropore volume (V_{DR} (N_2)) and ultramicropore volume (V_{DR} (CO_2)) were calculated by applying the Dubinin-Radushkevich (DR) method[32] in the relative pressure ranges of 10^{-6}– 0.1 and 10^{-5} – 0.03 of the N_2 and CO_2 isotherms, respectively. The total pore volume (V_T) was calculated as the amount of N_2 adsorbed at the relative pressure of 0.95 assuming that it is in liquid form. The mesopore volume (V_{mesop}) was obtained as the difference between V_T and V_{DR} (N_2).The DFT method, applied to the N_2 adsorption branch, was used to obtain the pore size distributions (PSDs). In the case of the carbon materials the QSDFT method developed by Quantachrome[33] was applied since this method eliminates the artificial minimum at 1 nm introduced by NLDFT modelling assumptions.[33, 34] Besides of PSDs, different pore volume parameters were obtained from the QSDFT cumulative pore volume data.

2.3. Electrochemical performance measurements

The electrical conductivity of the samples was measured using a homemade Teflon cylindrical mold with an area (A) of 1.1 cm^2 and 100 mg of sample. The load and the sample length (d) were measured using two stainless steel plungers. The resistance (R) of the powdered materials, without any binder or conductive additive, was measured between the two plungers. The applied current was 0.5 A and the voltage was registered at different load pressures. The conductivity was calculated as $\sigma = {}^{d}/_{RA}$.

The electrochemical tests were carried out by using a three-electrode beaker-type cell in 1M H_2SO_4 and with an Ag/AgCl saturated KCl reference electrode (BAS Inc., Japan). A paste was prepared by mixing the carbon sample with polytetrafluoroethylene (PTFE 6-J, Du Pont-Mitsui Fluorochemicals Company, Ltd.) as binder and carbon black in a ratio 90:5:5 respectively. The working electrode was prepared by sandwiching an 8 mg sheet made out of the paste in a stainless steel mesh (SUS 304 100 mesh, Nilaco Corp.) and pressed at 20 MPa for 1 minute. The counter electrode was made in the same manner but using 10 mg of paste prepared with an activated carbon fiber (A20) as active material. The working and counter electrodes were arranged in a stack, separated by a cellulose separator (TF-4850, Tokyo Sangyo Yoshi Co. Ltd.). The stack was soaked in the electrolyte, vacuum-degassed for 1h and kept at 40 ºC for 3 days. Nitrogen gas was bubbled in the electrolyte for 30 min prior to the measurements. Cyclic voltammetry (potential window: [-0.1, 0.8] V vs. Ag/AgCl) and electrochemical impedance spectroscopy (frequency range: [10^{-2}-10^{-5}] Hz) measurements were carried in a Biologic VMP3 potentiostat.

3. Results and discussion

3.1. Textural and structural characterization

Table 1. Pore textural parameters deduced from the N_2 and CO_2 adsorption isotherms for C and CB series of chemically activated carbons at different KOH/OMC ratios and activation temperatures.

Sample	S_{BET} (m^2/g)	V_T (cm^3/g)	V_{mesop} (cm^3/g)	DR method		QSDFT method		
				V_{DR} (N_2) (cm^3/g)	V_{DR} (CO_2) (cm^3/g)	$V_{p< 1\ nm}$ (cm^3/g)	$V_{p<2\ nm}$ (cm^3/g)	$V_{2 < p < 50\ nm}$ (cm^3/g)
C	341	0.53	0.40	0.13	0.05	0.01	0.05	0.46
C21-850	960	0.76	0.34	0.42	0.19	0.21	0.34	0.38
C41-750	1028	1.00	0.58	0.42	0.20	0.20	0.34	0.61
C41-850	982	0.60	0.16	0.44	0.28	0.23	0.39	0.17
CB21-850	618	0.75	0.51	0.24	0.12	0.08	0.16	0.56
CB41-750	634	0.75	0.50	0.25	0.11	0.08	0.16	0.57
CB41-850	1247	1.19	0.67	0.52	0.20	0.23	0.42	0.73
CB81-750	1124	1.10	0.64	0.46	0.23	0.21	0.35	0.70
CB81-850	1757	1.64	0.93	0.71	0.25	0.29	0.52	1.04

Sample C yields a type IV isotherm (see Fig. 1S), characteristic of a mesoporous material. Activated OMCs produce type IV isotherms (in the medium and high P/P_0 ranges) with some contribution of type I (in the low P/P_0 range). This indicates that activation produces micropore development, while the mesoporous structure is conserved to some extent, with the exception of sample C41-850 which yields a type I isotherm (Fig. 1S). Textural parameters of the C and CB carbon series are displayed in Table 1. In general, lower micropore volumes are obtained from the QSDFT method than form the DR method. Nevertheless, the same evolution of both micro and mesoporosity with the activation conditions is observed, despite the different methods and adsorbates used. Thus, the specific surface area, S_{BET}, and the micropore volumes increase progressively with increasing activation temperature and/or KOH/OMC ratio for both carbon series. Specific surface areas are, excepting CB21-850and CB41-750, around 1000 m^2/g for all activated OMCs. CB carbons activated in mild conditions present a limited microporosity development due to the silica template reaction with the KOH.[23] Actually, we previously demonstrated that a part of the KOH is consumed reacting with the silica instead of with the carbon, which decreases the amount of activating agent available for the development of the porosity specially at low KOH/OMC ratios.[23] Thus, C41-750 and CB41-750, which were activated in analogous conditions, exhibit large differences in their micropore volumes. This is not the case for strong activation conditions (high KOH/OMC proportions and high activation temperatures) since high surfaces areas are achieved for both C and CB carbon series regardless of the silica template presence. The mesopore volume, $V_{2<p<50nm}$, increases from 0.46 cm^3/g for the initial OMC (C sample) to 0.6 or 1.0 cm^3/g for the activated carbons in C and CB series, respectively. It is worth pointing out the drastic decrease in mesopore volume (0.17 cm^3/g) that is observed for C41-850. This fact reveals the collapse of the ordered mesoporous structure for strong activation conditions in the C series, as was demonstrated in our previous work.[22] On the contrary, when the activation is performed in the presence of the silica template (CB series), a large conservation of the mesopore volume occurs. Thus, for strong activation conditions important differences in the mesopore volume between both series are observed.

Fig. 1 displays the pore size distributions for the C (Fig. 1a) and CB series (Fig. 1b) calculated by the QSDFT method from the nitrogen adsorption-desorption isotherms at -196 ºC. The initial carbon (C, Fig. 1a) has a narrow mesopore size distribution, centered at 3.4 nm. As regards C series, C41-750 and C21-850 present maxima between 0.5-1.5 nm and 3.4 nm, whereas C41-850 exhibits a strong maximum at 0.9 nm with no presence of peaks in the mesopore range. This fact agrees with the above-commented decrease in the mesopore volume for C series activated under strong conditions (Table 1). On the other hand, carbons from the CB series also exhibit a narrow pore size distribution in the mesopore range (maxima at 3.4 nm); micropores(centered at 0.9 and 1.5 nm) are progressivelly generated along the series as the activation conditions become stronger. Even under the harshest activation conditions (CB81-850), CB carbons present a bimodal pore size distribution revealing a remarkable conservation of the ordered mesostructure when the activation is carried out in the presence of the silica template.

The narrow microporosity of the carbons was evaluated by CO_2 adsorption at 0 ºC and the obtained isotherms are displayed in Fig. 2. Complementarily, the volume of pores < 1 nm in width was determined from the cumulative pore volume obtained by the QSDFT method. The C carbon presents a very low CO_2 uptake and a quasi-linear isotherm, indicating the absence of narrow microporosity (see its very small values of V_{DR} (CO_2) and $V_{p<1nm}$ in Table 1). On the other hand, activated OMCs (both C and CB series) yield higher CO_2 uptakes, which increase gradually with increasing KOH/OMC proportion and activation temperature (see V_{DR} (CO_2) and also $V_{p<1nm}$ data in Table 1). Samples prepared under the strongest activation conditions exhibit the highest difference between their

micropore volume and narrow micropore volume (see the difference between V_{DR} (N_2) or $V_{p<2nm}$ and V_{DR} (CO_2) or $V_{p<1nm}$ in Table 1), which indicates that widening of micropores takes place. This can also be observed from the change in shape of CO_2 isotherms, where the CO_2 uptakes at the lower relative pressures clearly decrease (see CB81-850 isotherm in Fig. 2).

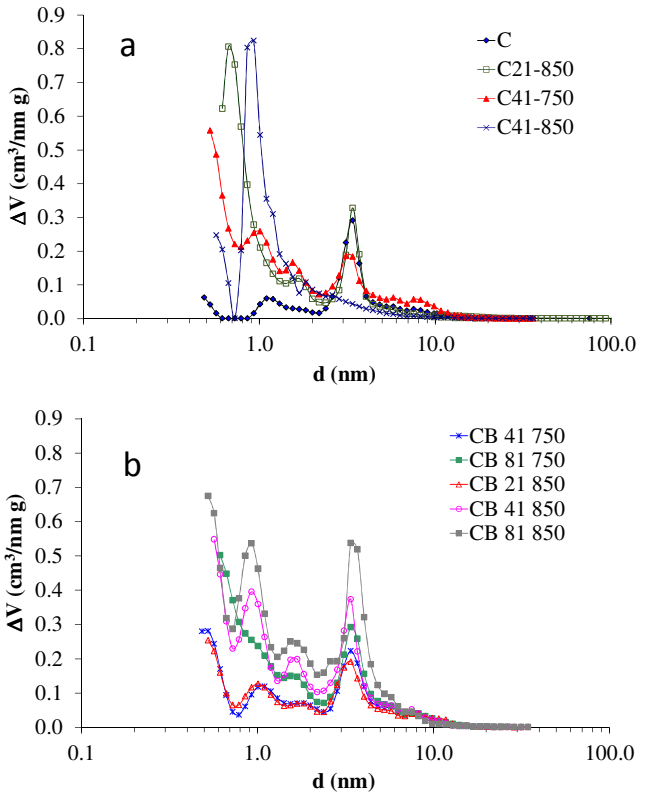

Fig. 1.PSDs calculated by applying the QSDFT method to the N_2 adsorption isotherms at -196 ºC for a) C series and b) CB series.

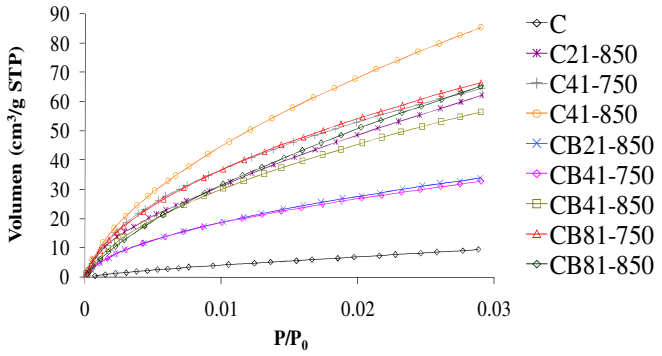

Fig. 2.CO_2 adsorption isotherms at 0ºC for theC and CB series of chemically activated carbons at different KOH/OMC ratios and activation temperatures

Fig. 3 displays the low-angle X-ray diffraction patterns of the studied carbons. The non-activated OMC (sample C, Fig. 3a) gives three peaks at 2θ = 0.9, 1.6 and 1.8º, which can be indexed as (100), (110) and (200) diffraction planes. These peaks are typical for CMK-3 type carbons and they are associated to a p6mm hexagonal symmetry.[35] The carbons from the C series (Fig. 3a), except for C21-850, present a very weak and poorly-resolved (100) peak whereas those from the CB series display an intense and well-resolved (100) peak (Fig. 3b) and also the (110) and (200) peaks can be appreciated in this series. Fig. 3b confirms that, during the activation process, a significant conservation of the ordered mesostructure takes place in the CB series, while this does not occur for the C series (where the ordered mesostructure is clearly deteriorated). Noteworthy is the case of CB81-850 where a strong decrease in the (100) peak intensity and the disappearance of the (110) and (200) peaks indicate a considerable loss of the long range order. Considering all the obtained results, a different structural evolution for the C and CB carbon series under strong activation conditions is proposed in Fig. 4. The structure of CMK-3 type carbons is comprised of cylindrical rods (coming from the replica of the SBA-15 mesoporous channels) linked by tiny bars (coming from the infiltration of the micropores that connect the primary mesoporous channels of this silica).[36] Thus, the mesoporous character of this type of carbons lies in the inter-rod periodic distances. The carbons from the C series undergo a deterioriation of the supporting bars placed between the long rods during the activation process. This leads to a partial collapse of the ordered mesoporous structure. This collapse yields a carbon formed by cilindrical rods without mesopores between them, which can be squematiced similarly to the carbon obtained from the infiltation of the MCM-41 silica.[37, 38] MCM-41 silica has an hexagonal structure formed by cilindrical mesopores (like SBA-15) but, without micropores connecting these primary mesporous chanels. Therefore, this silica yields cilindrical rods after carbon infiltration and not mesoporous carbons.[37, 38] On the contrary, the carbons from the CB series retain their mesoporous character after the activation process thanks to the presence of the silica template during the activation, which protects the supporting tiny bars from the KOH attack.

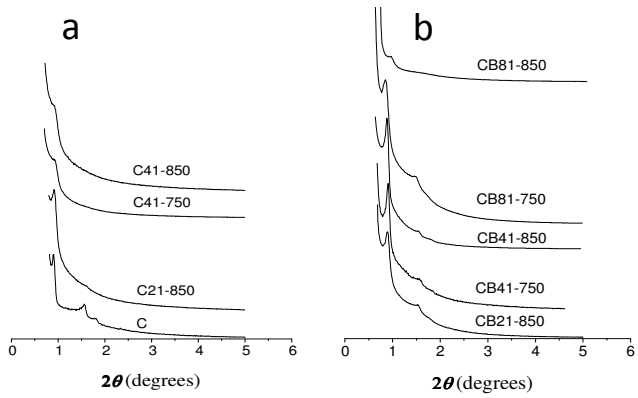

Fig. 3. Low-angle XRD patterns corresponding to the original and activated OMCs in the C and CB series.

By way of illustration, the TEM images of CB41-850 (a) and C41-850 (b) samples are included in Fig. 4 (SEM and TEM images for a selection of samples are shown in Fig. 2S). Carbons activated after template removal (C series, Fig. 4b) led

to disordered structures while carbons activated in template presence (CB series, Fig. 4a) present a high mesoscopic order with clear mesoporous channels and carbon rods (7 nm in width) periodically arranged with an inter-rod distance about 3.4 nm.

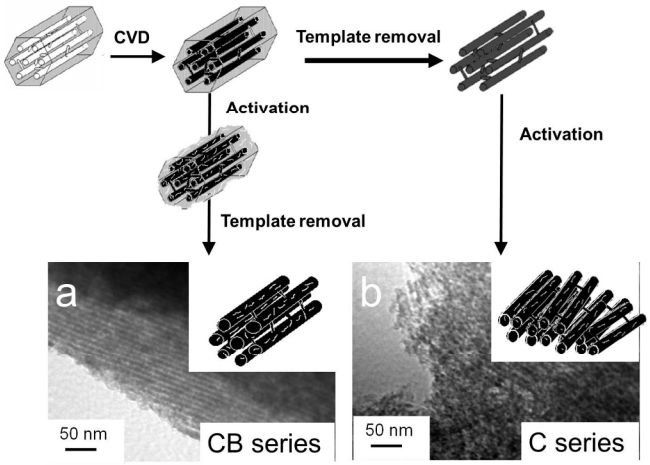

Fig.4. Schemefor the proposed structure of the micro-mesoporous carbon obtained by chemical activation of the carbon/silica composite (CB series) and of the OMC (C series). TEM images of CB41-850 (a) and C41-850 (b) samples.

3.2. Electrochemical performance

Fig.5 shows the cyclic voltammetry curves obtained by using C and CB carbon series as active materials of working electrodes in a three-electrode type cell. For low-scan rates (5 mV/s), both C (Fig. 4a) and CB series (Fig. 4b) yields quasi-rectangular voltammograms with a reversible peak centered at 0.4 V vs. Ag/AgCl most probably due to the quinone/hydroquinone redox couple typical for carbon materials.[10] The OMCs capacitance is highly increased after the KOH activation mainly due to the rise in the specific surface area (see Table 1). In this sense, samples CB41-850 and CB81-850 present lower capacitances than expected. This can be explained by the fact that these samples present a wider PSD in the micropore region (see Fig. 1) and a low contribution of the narrow microporosity to the total porosity (see Table 1). On this basis, CB81-850 should be the sample exhibiting the highest specific capacitance. However, comparing with the other samples, this material has a wider micropore size distribution as explained previously (see Fig. 1 and 2). This could worsen its electrochemical performance since it has been widely demonstrated that both the micropore size distribution and the average micropore size[39, 40] are very decisive in the electric double layer formation.

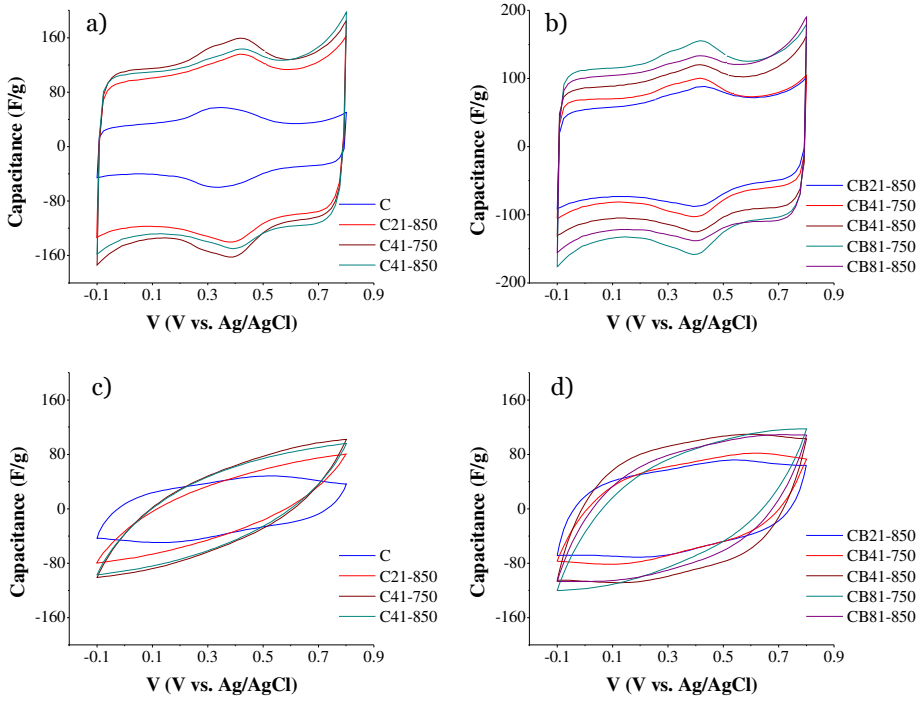

Fig.5. Cyclic voltammograms for carbon samples at 5 mV/s (a and b) and 500 mV/s (b and c) in 1M H_2SO_4.

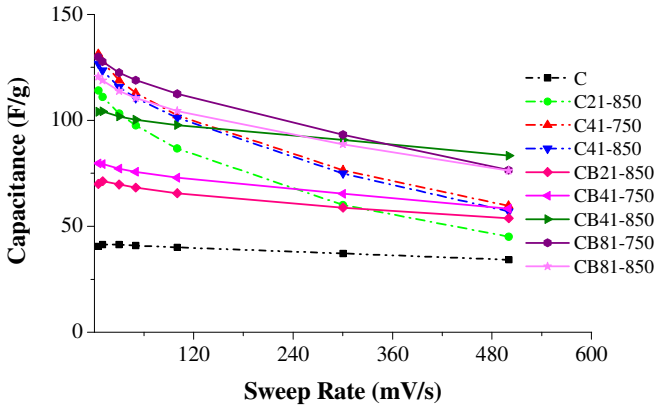

Fig.6. Dependence of capacitance on sweep rate.

At high sweep rate (500 mV/s) the materials show highly distorted voltammograms (see Fig. 5 c and d), which is indeed a common feature for carbon materials.[14, 41] The voltammograms are very similar to each other for the samples of the C series regardless of the pore size distribution in the mesopore range; notice for instance that samples C41-750 and C41-850 exhibit almost identical cyclic performances at low and high sweep rates although they have very different mesopore size distributions (see Fig. 1a). Therefore, the order degree of the mesoporous structure is an important factor for the electrochemical performance. In this way, the carbons from the CB series show more rectangular-shaped CV curves than those form the C series at the highest sweep rate used in this study (Fig. 5d), revealing a good performance and low resistance for electrolyte diffusion. Even CB81-750 and CB81-850, which present some cycle distortion, have higher capacitance than the carbons from the C series. Therefore, CB carbons exhibit a better capacitive behavior at high voltage sweep rates due to a low mass transfer resistance. This could be explained by the fact that the electrolyte path is uniform and simple due to the periodicity and order of the mesoporous structure.

The relationship between the capacitance and the voltage scan rate has been plotted in Fig. 6. The specific capacitances were calculated from the voltammograms as $C_r = \frac{1}{2rV_w}\int_{V_0}^{V_1} I(V)dV$, where r is the sweep rate and V_w is the window voltage. The different behavior of the carbons under different sweep rate, commented above (Fig. 5c and 5d), is easily observed since the specific capacitance in the C carbon series remarkably decreases with increasing sweep rate. On the other hand, the evolution of the capacitance as a function of the sweep rate of sample C and the samples from the CB series is much more stable, with high capacitance retention. However, the CB 81 samples loose capacitance at almost the same rate as those from the C series. The mesoscopic order of CB81 samples is slightly more damaged than in the other samples of the CB series (see Fig. 3), becoming more similar to the case the C series samples, which explains their different behavior. Thus, the samples from the C series retain about 45% of the capacitance (calculated as the C_{500}/C_5ratio); this value increases for the CB81 series up to approximately 60% and it is remarkably larger for sample C and the other samples from the CB series, which yield values around 80%. This evolution is in good agreement with the preservation of the mesoscopic order.

Electrochemical impedance spectroscopy was employed to further quantify the influence of the mesostructure order on the electrochemical performance. The resistance values of the electrodes are listed in Table 2. R_S stands for the sum of the resistances in the electrodes, obtained from the high frequency limit and R_D is the resistance related to the diffusion of the electrolyte ions in the active materials of the electrodes, calculated from the low-frequency region of the spectra.[42] R_S is very similar for all the electrodes since all of them were built in the same manner. However, the diffusion resistance is considerably higher in the case of the KOH-activated C series of samples. This indicates that the samples presenting mesostructure deterioration have a much larger resistance to electrolyte diffusion within the electrode porosity. As mentioned above, the access of the electrolyte ions to the bulk of the active material in the electrodes is much less intricate in the case of the ordered samples (see Fig. 4).

Table 2. Specific capacitances and resistance of the electrodes prepared from the C and CB series and electrical conductivity of the powdered samples.

Sample	C_5 (F/g)[a]	R_S (Ω)[b]	R_D (Ω)[b]	σ (S/cm)[c]
C	41	0.14	0.52	8.54
C21-850	114	0.18	0.83	3.45
C41-750	131	0.16	0.59	2.44
C41-850	127	0.17	0.64	2.30
CB21-850	70	0.18	0.29	6.79
CB41-750	80	0.18	0.34	3.03
CB41-850	104	0.17	0.29	4.26
CB81-750	130	0.16	0.47	2.77
CB81- 850	121	0.18	0.38	2.85

a: Calculated from the CV voltammograms at 5 mV/s.
b: Calculated from the electrochemical impedance spectroscopy measurements.
c: electrical conductivity at ca. 20 MPa

The capacitance dependence on the frequency (calculated from the impedance spectroscopy as $C = -Z_{im}/2\pi f|Z|^2$) [43]is shown in Fig.7. Sample C and the samples from the CB series show a fairly stable capacitance in the 0.01-0.2 Hz region, which is indicative of a good capacitive behavior at the electrolyte/carbon interface.[44] The drop of the capacitance with increasing frequency starts at lower frequencies for the CB81 samples than for other carbons from the CB series and, in the case of the C carbon series, the capacitance significantly decreases even in the low frequency range and the drop takes place at lower frequencies. Improvement in the low-frequency

capacitive performance has been ascribed to the presence of the mesopores,[45] but in this case it is expected that the better order at a mesoscopic level may also have an important influence on the performance.

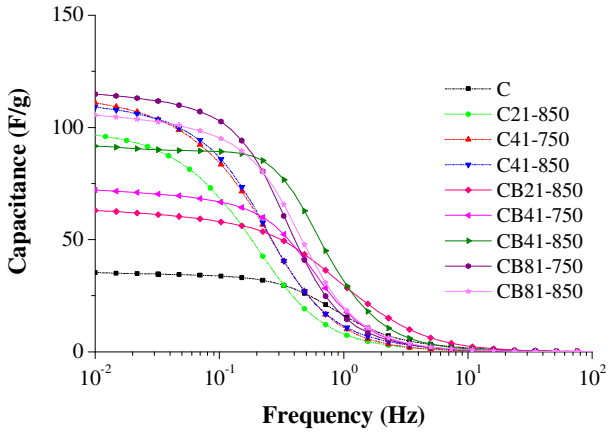

Fig. 7. Capacitance evolution with the frequency at 0 V vs. Ag/AgCl in 1M H_2SO_4.

The electrical conductivity of the samples was measured in the absence of either binder or conductive additive (see Table 2 and Fig. 3S). The values obtained for the KOH-activated samples were in the range 2.30-4.26 S/cm (at ca. 20 MPa) with the exception of sample CB21-850, in which mild activation conditions were used so the structure is similar to that of the non-activated sample, C. Even though the values lie in a relatively narrow range there is a difference in the conductivity of the samples. However, the conductivity values do not correlate with the electrochemical performances. For instance, sample C21-850 shows a slightly higher conductivity than CB41-750 but the electrochemical performance of the latter sample is better even though the surface area and micropore volumes are higher in the case of sample C21-850. Therefore, the different electrochemical behaviors associated with the mesostructural order observed in this study cannot be simply ascribed to differences in the conductivity of the samples.

Conclusions

For low scan rates, the capacitance is correlated to the specific surface area and pore size distribution, and no relationship with the degree of structural order in the electrode material is observed. On the contrary, for high scan rates the behavior as active material in EDLC electrodes is greatly enhanced by the order degree of the mesostructure of the carbons. Thus, hierarchical micro-mesoporous carbons presenting a highly-ordered mesostructure show a very good durability and good performance at high sweep rates when used as electrode materials. Consequently, it has been demonstrated that a highly-ordered and interconnected mesoporous system substantially enhances the diffusion of electrolyte ions within the bulk of the electrode active materials. As it has been widely demonstrated, the presence of mesopores is beneficial for the electrochemical performance of porous carbons, but, in this work we have demonstrated as well the decisive importance of their order degree. The obtained carbons provide almost constant capacitance values regardless of the applied sweep rate. This can lead to a fast charge/discharge capability, which is an important requirement for real implementation and is recognized as one of the main advantages in EDCLs.

Acknowledgements

The authors gratefully acknowledge the Spanish Ministerio de Ciencia e Innovación (project MAT2009-11375) and Ministerio de Economía y Competitividad and FEDER (project MAT2012-34011) for financial support.

Notes and references

[a]Instituto Nacional del Carbón, INCAR-CSIC, Apartado 73, 33080 Oviedo, Spain. *E-mail: marina@incar.csic.es.
[b]Institute of Multidisciplinary Research for Advanced Materials, Tohoku University, Aoba-ku, Sendai 980-8577, Japan.

ElectronicSupplementaryInformation (ESI) available: N_2adsorption-desorptionisotherms, SEM and TEM imagesfor a selection of samples, conductivity as a function of loadingpressureforthe C and CB series. See DOI: 10.1039/b000000x/

1. M. Winter and R. J. Brodd, *Chem. Rev.*, 2004, **104**, 4245-4270.
2. R. Mysyk, E. Raymundo-Piñero and F. Béguin, *Electrochem. Commun.*, 2009, **11**, 554-556.
3. L.-h. Wang, M. Toyoda and M. Inagaki, *New Carbon Mater.*, 2008, **23**, 111-115.
4. Y. Li, Z.-Y. Fu and B.-L. Su, *Adv. Funct. Mater.*, 2012, **22**, 4634-4667.
5. H. Nishihara and T. Kyotani, *Adv. Mater.*, 2012, **24**, 4473-4498.
6. Y. Zhai, Y. Dou, D. Zhao, P. F. Fulvio, R. T. Mayes and S. Dai, *Adv. Mater.*, 2011, **23**, 4828-4850.
7. T.-c. Chou, C.-h. Huang, R.-a. Doong and C.-c. Hu, *J. Mater. Chem. A*, 2013, **1**, 2886-2895.
8. A. G. Pandolfo and A. F. Hollenkamp, *J. Power Sources*, 2006, **157**, 11-27.
9. X.-L. Wu and A.-W. Xu, *J. Mater. Chem. A*, 2014.
10. E. Frackowiak, *Physical Chemistry Chemical Physics*, 2007, **9**, 1774-1785.
11. Y. Lv, F. Zhang, Y. Dou, Y. Zhai, J. Wang, H. Liu, Y. Xia, B. Tu and D. Zhao, *J. Mater. Chem.*, 2012, **22**, 93-99.
12. K. S. Xia, Q. M. Gao, J. H. Jiang and J. Hu, *Carbon*, 2008, **46**, 1718-1726.
13. W. Xing, C. C. Huang, S. P. Zhuo, X. Yuan, G. Q. Wang, D. Hulicova-Jurcakova, Z. F. Yan and G. Q. Lu, *Carbon*, 2009, **47**, 1715-1722.
14. E. Frackowiak and F. Beguin, *Carbon*, 2001, **39**, 937-950.
15. H. Itoi, H. Nishihara, T. Kogure and T. Kyotani, *J. Am. Chem. Soc.*, 2011, **133**, 1165-1167.
16. G. Sun, J. Wang, X. Liu, D. Long, W. Qiao and L. Ling, *J. Phys. Chem. C*, 2010, **114**, 18745-18751.
17. L. Wang, Y. Zhou and J. Qiu, *Microporous Mesoporous Mat.*, 2013, **174**, 67-73.

18. T. Matsui, S. Tanaka and Y. Miyake, *Adv. Powder Technol.*, 2013, **24**, 737-742.
19. H. Liu, Y. Zhang, Q. Ke, K. H. Ho, Y. Hu and J. Wang, *J. Mater. Chem. A*, 2013, **1**, 12962-12970.
20. Z. Wu, W. Li, Y. Xia, P. Webley and D. Zhao, *J. Mater. Chem.*, 2012, **22**, 8835-8845.
21. Y. Liang, Z. Li, X. Yang, R. Fu and D. Wu, *Chem. Commun.*, 2013, **49**, 9998-10000.
22. M. Enterría, F. Suárez-García, A. Martínez-Alonso and J. M. D. Tascón, *Microporous Mesoporous Mat.*, 2012, **151**, 390-396.
23. M. Enterría, F. Suárez-García, A. Martínez-Alonso and J. M. D. Tascón, *Carbon*, 2012, **50**, 3826-3835.
24. M. Choi and R. Ryoo, *J. Mater. Chem.*, 2007, **17**, 4204-4209.
25. J. Gorka, A. Zawislak, J. Choma and M. Jaroniec, *Carbon*, 2008, **46**, 1159-1161.
26. J. Choma, J. Gorka, M. Jaroniec and A. Zawislak, *Top. Catal.*, 2010, **53**, 283-290.
27. J. Jin, S. Tanaka, Y. Egashira and N. Nishiyama, *Carbon*, 2010, **48**, 1985-1989.
28. K. S. Xia, Q. M. Gao, S. Q. Song, C. D. Wu, J. H. Jiang, J. Hu and L. Gao, *Int. J. Hydrogen Energy*, 2008, **33**, 116-123.
29. M. Sevilla and A. B. Fuertes, *J. Colloid Interface Sci.*, 2012, **366**, 147-154.
30. X. Wang, J. S. Lee, C. Tsouris, D. W. DePaoli and S. Dai, *J. Mater. Chem.*, 2010, **20**.
31. K. S. Xia, Q. M. Gao, C. D. Wu, S. Q. Song and M. L. Ruan, *Carbon*, 2007, **45**, 1989-1996.
32. F. Rouquerol, J. Rouquerol and K. W. S. Sing, *Adsorption by Powders & Porous Solids. Principles, Methodology and Applications*, Academic Press New York, 1999.
33. A. V. Neimark, Y. Lin, P. I. Ravikovitch and M. Thommes, *Carbon*, 2009, **47**, 1617-1628.
34. J. P. Olivier, *Carbon*, 1998, **36**, 1469-1472.
35. S. Jun, S. H. Joo, R. Ryoo, M. Kruk, M. Jaroniec, Z. Liu, T. Ohsuna and O. Terasaki, *J. Am. Chem. Soc.*, 2000, **122**, 10712-10713.
36. M. Impéror-Clerc, P. Davidson and A. Davidson, *J. Am. Chem. Soc.*, 2000, **122**, 11925-11933.
37. M. Kruk, M. Jaroniec, R. Ryoo and S. H. Joo, *J. Phys. Chem. B*, 2000, **104**, 7960-7968.
38. R. Ryoo, S. H. Joo, M. Kruk and M. Jaroniec, *Adv. Mater.*, 2001, **13**, 677-681.
39. B. Xu, S. Hou, H. Duan, G. Cao, M. Chu and Y. Yang, *J. Power Sources*, 2013, **228**, 193-197.
40. D. Hulicova-Jurcakova, M. Seredych, G. Q. Lu and T. J. Bandosz, *Adv. Funct. Mater.*, 2009, **19**, 438-447.
41. W. Xing, S. Z. Qiao, R. G. Ding, F. Li, G. Q. Lu, Z. F. Yan and H. M. Cheng, *Carbon*, 2006, **44**, 216-224.
42. E. Raymundo-Piñero, M. Cadek, M. Wachtler and F. Béguin, *ChemSusChem*, 2011, **4**, 943-949.
43. P. L. Taberna, P. Simon and J. F. Fauvarque, *J. Electrochem. Soc.*, 2003, **150**, A292-A300.
44. K. Jurewicz, C. Vix-Guterl, E. Frackowiak, S. Saadallah, A. Reda, J. Parmentier, J. Patarin and F. Beguin, *J. Phys. Chem. Solids*, 2004, **65**, 287-293.
45. C. Vix-Guterl, S. Saadallah, K. Jurewicz, E. Frackowiak, M. Reda, J. Parmentier, J. Patarin and F. Beguin, *Mater. Sci. Eng. B-Adv. Funct. Solid-State Mater.*, 2004, **108**, 148-155.